ACS APPLIED ENGINEERING MATERIALS

pubs.acs.org/acsaenm Article

Synergistic Mixing Effects on Electrical and Mechanical Properties in Homogeneous CNT/Cu Composites

Kosuke Tanaka, Takayuki Nakano, Yoshinobu Shimamura, and Yoku Inoue*

Cite This: ACS Appl. Eng. Mater. 2023, 1, 2359–2367 Read Online

ACCESS | Metrics & More | Article Recommendations | Supporting Information

ABSTRACT: A homogeneous composite of aligned carbon nanotubes (CNTs) and copper was fabricated by combining copper nanoparticle functionalization with the CNT dry-spinning technology. The copper nanoparticles decorating the CNTs enabled high-yield copper electroplating inside the CNT yarn. Our homogeneous CNT/Cu composite had a weight density 38% lower than copper, yet had a 2.8-fold lower-temperature coefficient of resistance (TCR), 3.6 times higher specific current capacity (ampacity), and almost the same specific conductivity. The high alignment of the CNTs and the firm contacts at the CNT/Cu interface contributed to maximizing the conductivity by inducing elastic scattering of free electrons, leading to lower TCR and higher specific ampacity. The firm contacts at the CNT/Cu interface also enabled effective load transfer between the CNTs and copper matrix and reinforced the tensile strength of copper by a factor of 3.7. The smaller TCR and reinforced tensile properties of the homogeneous CNT/Cu composite make it promising for thin, lightweight wiring materials for small, lightweight motors and coils.

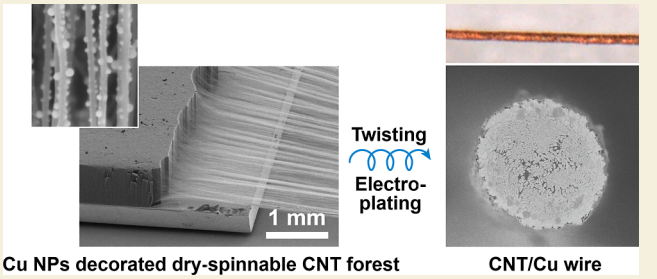

KEYWORDS: *carbon nanotubes, CNT/Cu composite, nanoparticles, electrical property, mechanical property*

1. INTRODUCTION

The automobile industry is switching from fossil fuel vehicles to electric vehicles.[1] The use of and demand for copper wiring, which is the most commonly used material for power transmission, are also increasing.[2,3] The increasing weight of copper wiring leads to lower fuel efficiency, so reducing the weight of the wiring material has become a priority. Consequently, a lightweight wiring material is needed to replace the copper wiring. Carbon nanotubes (CNTs), which have a current capacity thousands of times greater than that of metals, are a candidate alternative wiring material[4−6] because they are lightweight and have good electrical conductivity and high mechanical strength.[7,8]

With the development of CNT spinning, including dry spinning,[9,10] wet spinning,[11] and aerosol spinning techniques,[12] CNTs can now be made into long fibers, ranging from several meters to several kilometers in length, and are now commercially available. However, the electrical conductivity of CNT yarn is as low as several hundred to thousands of siemens per centimeter due to crystal defects in the CNTs, the contact resistance between CNTs, and non-negligible porosity.[13−19] Therefore, to use CNTs for power transmission, further improvements in conductivity are required to decrease power loss.

Several approaches for increasing the conductivity of CNTs have been reported. The Pasquali group has reported the use of highly conductive CNTs to increase the CNT fiber conductivity.[20] A high conductivity of 5×10^4 S cm^{-1} was achieved by closely packing chemically doped CNTs, although the use of CNTs with extremely high crystallinity was required. Another approach is to make a composite of CNT and copper.[21,22] The CNT/Cu composite material is expected to show both the high electrical conductivity of copper and the lightness and high strength of CNTs. Depositing copper on single-walled CNT sheets by electrolytic copper plating achieved a current capacity (ampacity) about 100 times higher than that of copper with the same conductivity.[23] However, it was obtained from a short gauge length of 50 μm, and the concern is that heat dissipation to the electrodes will adversely affect the increase in the ampacity.[24] To apply electroplating to wiring materials, it is necessary to understand the ampacity at longer wire lengths.

There are many studies on composite materials consisting of long CNT yarns and copper. However, in simple electroplating or physical deposition methods, the copper is mainly concentrated at the periphery of the yarn, resulting in a core-clad structure.[25−32] Therefore, there were no synergistic effects of the mixture of CNT and copper on the electrical and mechanical properties, and the electrical conductivity mainly

Received: May 21, 2023
Revised: August 17, 2023
Accepted: August 17, 2023
Published: August 30, 2023

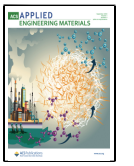

depended on the fraction of copper, whereas the tensile properties were strongly related to the CNT yarn. Recently, copper has been incorporated into the CNT fibers well by periodic reverse biasing[33] or preseeding Cu in the CNT yarn[34] in electroplating. However, the mechanism by which the temperature coefficient of resistance (TCR) of CNT/Cu composites becomes smaller than that of copper and the strengthening mechanism of the tensile properties have remained unexplored.

In this work, we developed a method for fabricating aligned CNT/Cu composites that have high ampacity, lower TCR, and better tensile properties than copper from a homogeneous mixture, and we clarified the synergistic mixing effects on charge transport and load transfer mechanism in the composites. Pre-decorated copper nanoparticles (Cu NPs) played a crucial role in not only inducing the effective precipitation of copper inside the yarn structure but also in forming firm contacts between the copper and CNT crystal interfaces that enhance the electrical and mechanical properties.

2. EXPERIMENTAL SECTION

2.1. Dry-Spinnable CNT Forest

Vertically aligned CNTs were grown on the substrate by a two-step floating catalyst chemical vapor deposition (CVD) method (Table S1 and Figure S1). The details of the synthesis method are described in our previous report.[35,36] In the first step, a solution of ferrocene, the catalyst precursor for CNTs, dissolved in ethanol was atomized by ultrasonic waves and transported onto a Si substrate in a CVD chamber using Ar as a carrier gas. Ferrocene was pyrolyzed at 700 °C on a Si substrate to form Fe nanoparticles in situ. In the second step, acetylene was supplied as the carbon source gas to grow CNTs at a temperature of 700 °C and a pressure of 2.4 kPa. To make the CNT forests longer while maintaining good dry spin capability, chlorine gas was also supplied during CVD.[10] CNTs with a diameter of 10 nm and a height of about 300 μm were grown.

2.2. Cu NP Decoration on CNTs

Cu NPs were deposited on the CNT surface in a CNT forest. Copper(II) acetylacetonate [$Cu(acac)_2$], which was the Cu NP precursor, and a spin-capable CNT forest were placed in a CVD chamber. NPs were deposited homogeneously throughout the forest at 400 °C and a pressure of 4.0 kPa for 15 min in Ar (Figure 1a). $Cu(acac)_2$ evaporated and diffused into the CNT forest. The Cu NPs were nucleated by thermal decomposition on the CNT surface. Because the $Cu(acac)_2$ vapor diffuses homogeneously into the CNT forest, the Cu NPs are uniformly deposited over the forest, as shown in Figure S2. The density of the Cu NPs deposited on the CNTs was controlled by varying the $Cu(acac)_2$ loading.

2.3. Fabrication of Yarn with NP-Decorated CNTs

The continuous network of CNT bundles (CNT web) was drawn out continuously from the edge of the CNT forest. The CNT yarn was fabricated by twisting the CNT web (Figure S3). The rotational speed of the spindle was 14,000 rpm, and the drawing speed was 50 mm s^{-1}.[10,37]

2.4. Electrolytic Copper Plating

To precipitate copper on CNTs, CNT-twisted yarns with and without Cu NPs were electroplated using copper sulfate solution (Table S2). With the CNT yarn functioning as a cathode, DC electroplating was performed (Figure S4). The deposition voltage was adjusted in the range of 2.2 to 4.4 V depending on the yarn size to maintain a current density of 0.2 A dm^{-2} for 2 h. Then, to reduce the copper oxide and smooth the adhesion between the CNTs and copper, the CNT/Cu samples were heated at 700 °C for 1 h with Ar (400 sccm) and H_2 (100 sccm) flowing at a pressure of 66.5 kPa.

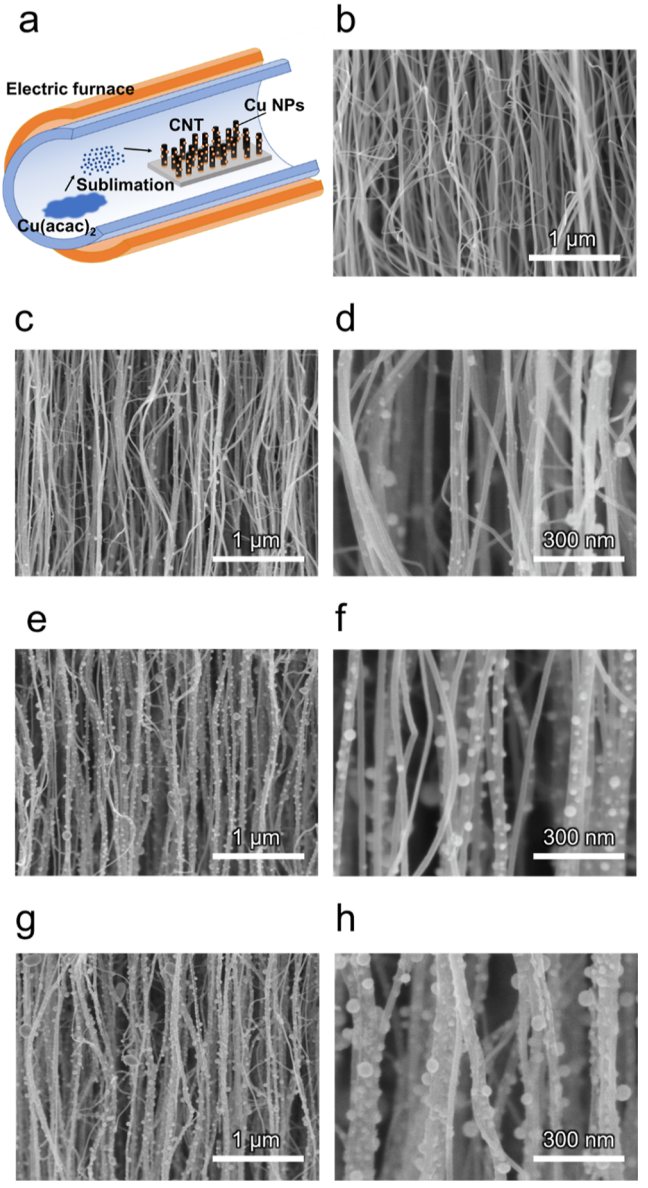

Figure 1. (a) Schematic of Cu NP deposition on a CNT forest. SEM images of the CNT forest (b) before Cu NP deposition and Cu NPs deposited forests using (c) 10, (e) 30, and (g) 100 mg of $Cu(acac)_2$. Magnified images of (c,e,g) are shown in (d,f,h), respectively.

2.5. Characterization

The CNT/Cu structures were observed by scanning electron microscopy (SEM; SU-8030, Hitachi) at an acceleration voltage of 3 kV, emission current of 10 μA, and dwell time of 16.3 μsec. A smooth cross-section of the CNT/Cu wire was cut with a cross-section polisher (IB-09020 CP, JEOL). The samples were cut with an Ar ion beam acceleration voltage of 4.5 V and an ion beam current of 35 μA for more than 1 h. The small cutting speed condition resulted in a smooth surface with no redeposition on the cross-section. The interfacial structure between CNTs and Cu was observed in detail by transmission electron microscopy (TEM; JEM-2100F, JEOL) at 200 kV. TEM observations were made in the CNT alignment direction and orthogonal direction. Wire-shaped samples were thinned to about 80 nm by mechanical polishing and focused ion beam thinning for observation. Elemental analysis of the CNT/Cu composite was performed by energy-dispersive X-ray spectroscopy (EDS) during the SEM and TEM observations. Chemical species on the CNT sample surface were investigated by X-ray photoelectron spectroscopy (XPS; ESCA-3400, Shimadzu) measurements. Changes in crystal quality and

https://doi.org/10.1021/acsaenm.3c00269
ACS Appl. Eng. Mater. 2023, 1, 2359−2367

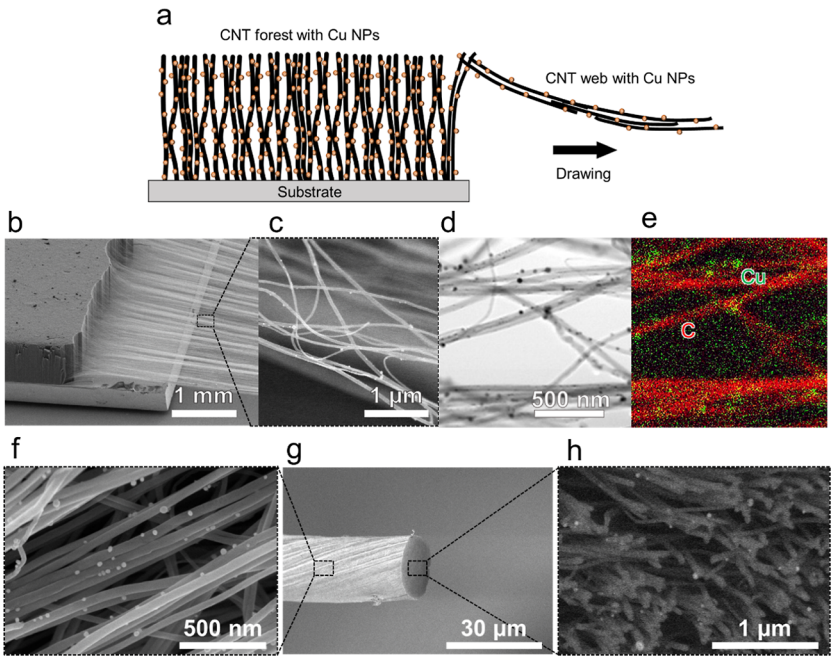

Figure 2. (a) Schematic of dry spinning of a CNT web from the CNT forest. (b) SEM image of dry spinning a web from the CNT forest and (c) high-magnification, (d) STEM, and (e) EDS images of Cu NP-decorated CNT web. The EDS spectrum is shown in Figure S5. (g) SEM image of CNT yarn and high-magnification images of (f) surface and (h) cross-section of the yarn.

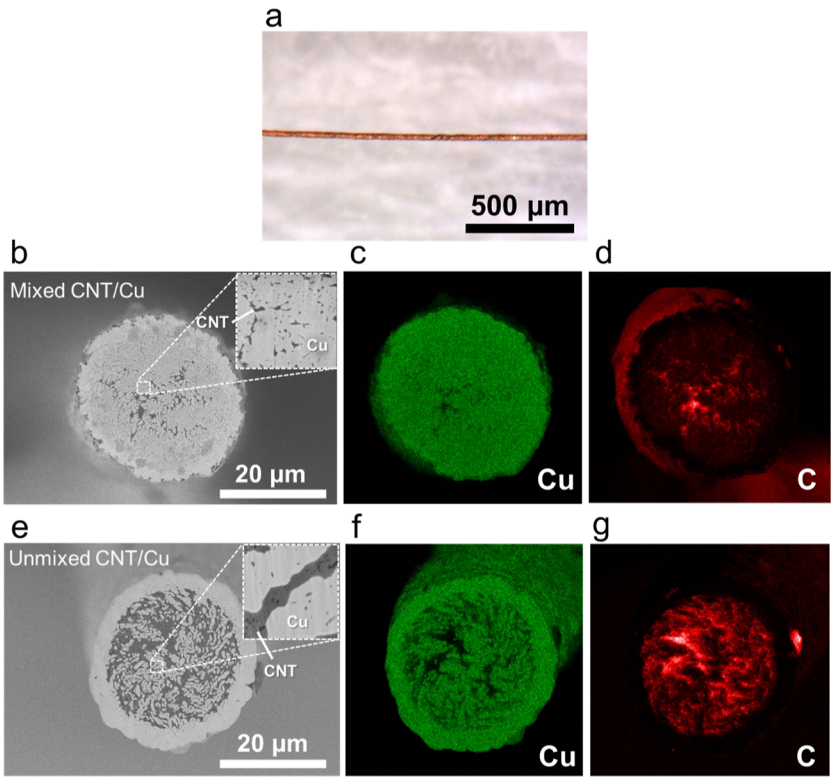

Figure 3. (a) Photograph, (b) SEM image, and EDS elemental maps of (c) copper and (d) carbon of the cross-section of an NP-decorated CNT/Cu wire. A cross-section of an undecorated CNT/Cu wire was also analyzed by (e) SEM and EDS maps of (f) copper and (g) carbon. Insets in the SEM images show magnified images of each cross-section.

strain of CNTs were analyzed by Raman scattering (XploRA, HORIBA) using an excitation wavelength of 532 nm.

The electrical conductivity was measured by four-terminal measurements under air. The ampacity was measured by two-terminal measurements under a high vacuum. The electrical properties were measured on three or more specimens. In the ampacity measurement, the measurement length was set to 10 mm to avoid heat exhaust to the electrodes due to the short measurement length. Ampacity was defined as the current density at which the samples broke. The tensile properties were measured using a tensile tester (EZ-L, Shimadzu) equipped with a non-contact extensometer (TRViewX, Shimadzu). The tensile strength and Young's modulus were the averaged values of

https://doi.org/10.1021/acsaenm.3c00269
ACS Appl. Eng. Mater. 2023, 1, 2359−2367

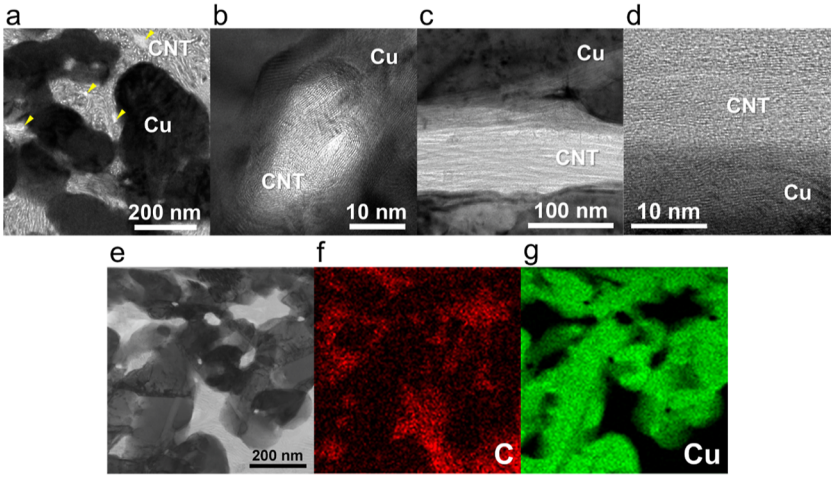

Figure 4. TEM images of the mixed CNT/Cu wire observed for the orthogonal cross-section at (a) low and (b) high magnification and for the parallel cross-section at (c) low and (d) high magnification. Elemental imaging of the orthogonal cross-section of the mixed CNT/Cu wire. (e) STEM image and EDS elemental maps of (f) copper and (g) carbon.

the measurements of the five test specimens. The gauge length was 10 mm, and the tensile speed was 0.05 mm min^{-1}.

3. RESULTS AND DISCUSSION

3.1. Cu NP-Decorated CNT Yarn Fabricated by Dry Spinning from a CNT Forest

The thermal deposition rate of Cu NPs varies depending on the pressure and temperature in the deposition chamber. Therefore, we first investigated the Cu NP deposition conditions to achieve homogeneous formation in the CNT forest while maintaining the dry spin ability; we found that NPs were deposited homogeneously throughout the forest at 400 °C and a pressure of 4.0 kPa, as shown in Figure S2. Figure 1c−h shows SEM images of CNT forests deposited with different densities of Cu NPs by varying the amounts of $Cu(acac)_2$ (10, 30, and 100 mg). An SEM image of a pristine CNT forest is also shown in Figure 1b for comparison. The deposition of NPs on individual CNTs was clearly observed (Figure 1c−h), and the number of NPs increased with the amount of $Cu(acac)_2$. For the CNT forests deposited with 10 and 30 mg of $Cu(acac)_2$, the high spin capability was also maintained. However, the loading of 100 mg of $Cu(acac)_2$ resulted in the deposition of a huge number of Cu NPs (Figure 1g,h), and many CNTs were connected by Cu NPs, allowing the entire CNT forest to form a strong linkage. Consequently, the CNT web could no longer be drawn out from the CNT forest, and dry spinning was impossible. For fabricating the CNT/Cu composites, a loading of 30 mg of $Cu(acac)_2$ was chosen to decorate Cu NPs for homogeneous, efficient electroplating of the CNT yarns.

At a loading of 30 mg of $Cu(acac)_2$, Cu NPs were uniformly deposited throughout the CNT forest (Figure 2a), and thus, the CNT webs drawn out by dry spinning were uniformly decorated with the NPs (Figure 2b). The high-magnification SEM (Figure 2c), scanning transmission electron microscopy (STEM) (Figure 2d), and corresponding EDS (Figure 2e) images revealed that Cu NPs were homogeneously deposited over the CNT web, which enabled the homogeneous incorporation of NPs into the twisted CNT yarn, as confirmed by SEM images of the yarn surface (Figure 2f), the yarn (Figure 2g), and the yarn cross-section (Figure 2h). CNT-twisted yarns have previously been fabricated by applying metallic colloidal NPs directly to CNT webs to make NP-functionalized CNT yarns.[38] The method was technically complex and needed a specialized system. In contrast, in our method, a simple dry process is used to deposit Cu NPs throughout the entire spin-capable CNT forest in advance, making it suitable for a wide range of applications, such as Cu NP-functionalized CNT forests, sheets, and twisted wires.

3.2. Structural Analysis of the CNT/Cu Wire

The CNT/Cu composite wire was fabricated by copper electroplating on the NP-decorated CNT yarn (Figure 3a). The surface of the CNT/Cu wire had a visible copper sheen. The cross-sectional SEM images of the copper-electroplated CNT yarn deposited with and without Cu NPs are shown in Figure 3b,e. The cross-sectional images show that the CNT/Cu wire with pre-deposited NPs on the CNTs had uniformly deposited copper from the periphery to the inside yarn. The high-magnification image shows that the copper was densely precipitated without apparent voids. The copper and carbon EDS mapping images, as shown in Figure 3c,d, confirm that the copper and CNTs were well mixed deep in the yarn. In contrast, the SEM and EDS images in Figure 3e−g show that the CNT/Cu wire without Cu NPs formed a core-clad structure with a large amount of copper precipitated at the periphery of the CNT yarn and many copper islands floating inside the yarn. This difference in Cu deposition indicated that the pre-deposition of Cu NPs on CNTs was effective for homogeneous mixing of the CNT/Cu system. Hereafter, homogeneous composite wires are referred to as mixed CNT/Cu wires and core-clad wires as unmixed CNT/Cu wires.

The presence of oxygen in the CNT surface area would also affect the Cu deposition rate. We have investigated the changes in the CNT surface state by decorating the CNT forest with Cu NPs using XPS measurements. As shown in Figure S6, we found similar degrees of C−O in the C 1s and O 1s signals for both samples modified with and without Cu NPs. Thus, it is strongly suggested that good Cu precipitation was derived from the decorated Cu NPs rather than the oxygen species.

Cu NPs play an essential role in accelerating copper deposition deep inside the CNT yarn, suggesting that there is an energetic benefit in depositing copper ions on Cu NPs rather than on CNTs. Because the distance between the CNT bundles in the CNT yarn was a few hundred nanometers, the

https://doi.org/10.1021/acsaenm.3c00269
ACS Appl. Eng. Mater. 2023, 1, 2359−2367

Table 1. Mean and Standard Deviation of Structural Data and Measured Electrical and Mechanical Properties of the CNT/Cu Wires, CNT Yarn, and Cu Wire

	weight density (g cm^{-3})	Cu volume fraction (%)	conductivity (S cm^{-1})	ampacity (A cm^{-2})	TCR (K^{-1})	tensile stress (MPa)	Young's modulus (GPa)
CNT yarn	0.56 ± 0.04	0	2.17 × 10^2 ± 63	1.50 × 10^4 ± 3.11 × 10^2	−0.6 × 10^{-3}	669 ± 10.6	32.3 ± 3.0
unmixed CNT/Cu	3.36 ± 0.42	33.4 ± 5.0	3.14 × 10^4 ± 1.12 × 10^4	7.22 × 10^4 ± 1.90 × 10^4	2.0 × 10^{-3}	184 ± 9.1	25.8 ± 6.5
mixed CNT/Cu	5.31 ± 0.27	56.7 ± 3.3	1.73 × 10^5 ± 4.82 × 10^4	1.26 × 10^5 ± 3.82 × 10^3	1.2 × 10^{-3}	699 ± 26.2	70.4 ± 5.9
Cu wire	8.94	100	4.35 × 10^5	5.82 × 10^4	3.3 × 10^{-3}	191 ± 4.9	83.5 ± 2.2

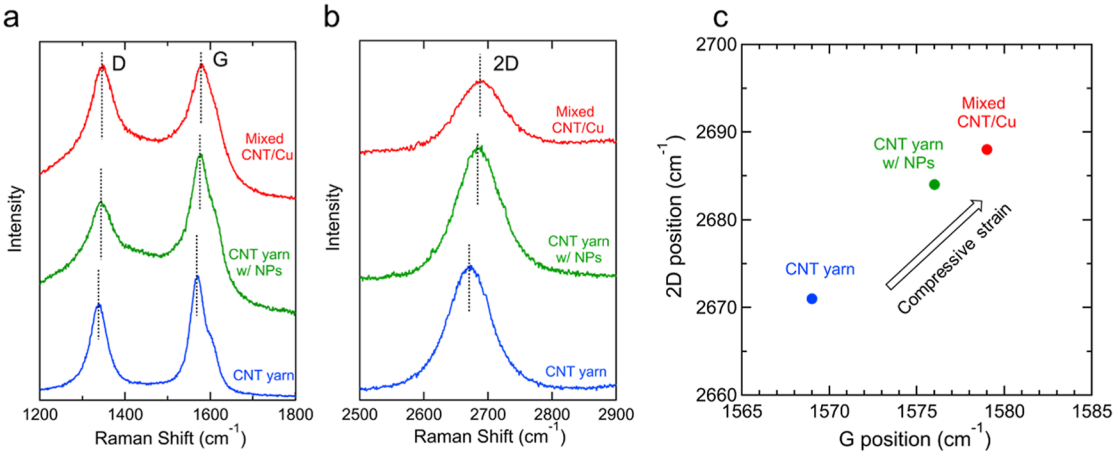

Figure 5. Raman spectra of the mixed CNT/Cu wire, NP-decorated CNT yarn, and twisted CNT yarn. Peak positions of (a) D and G, and (b) 2D modes of the wires were compared. (c) Relationship between the frequencies of the G and 2D modes of the wire samples.

copper ions may have diffused sufficiently in the entire yarn before the current was applied. The low current density in electroplating may have also contributed to the ions diffusing into the yarn instead of accumulating on the periphery.

The TEM image of the orthogonal cross-section of the mixed CNT/Cu wire is shown in Figure 4a. Copper precipitated between the CNT bundles. Cu NPs formed the growth nuclei, and the copper appeared to extend from there as a starting point. Therefore, nanovoids of several tens of nanometers were also formed between the bundles, as indicated by the yellow markers in Figure 4a. The parallel cross-sectional observation showed that copper precipitation occurred continuously in the longitudinal direction of the CNTs (Figure 4c). The higher-magnification images of the center of the wire revealed that the copper crystals were tightly deposited on the CNT surface (Figure 4b,d). TEM-EDS images of the orthogonal cross-section showed that the mixed CNT/Cu wire was composed of CNTs and copper and that copper precipitated in the center of the wire (Figure 4e−g).

Because the voids in the CNT/Cu wire were negligibly tiny, we calculated their volume ratios, assuming that the composite consisted only of CNTs and copper. The volume of copper was first estimated from the weight gain due to copper electroplating. The copper volume was then subtracted from the measured CNT/Cu wire volume to obtain the CNT volume, and the respective volume ratios were obtained. The volume ratios of copper in the CNT/Cu wires are shown in Table 1. In the mixed CNT/Cu wire with a weight density of 5.31 g cm^{-3}, copper constituted 56.7% of the total volume; thus, the composite material was a homogeneous mixture of CNTs and copper in comparable proportions.

We investigated strain induced in the CNTs near the CNT/Cu interface by Raman scattering measurements. An excitation laser illuminated the parallel cross-section of the mixed CNT/Cu wire and the surface of the CNT yarn containing Cu NPs. For comparison, an as-twisted CNT yarn was also measured. Figure 5 compares the position of the D, G, and 2D Raman modes of CNTs at 1340, 1575, and 2680 cm^{-1}, respectively. The positions of the G mode shifted toward higher frequencies in the order CNT yarns < NP-decorated yarns < mixed CNT/Cu wire (Figure 5a). A similar trend was also observed in the spectra of the 2D modes (Figure 5b). The relationship between the G and 2D frequency change is plotted in Figure 5c. As the copper covering the CNT surface and the CNT/Cu interfacial area increased, the G-2D relationship shifted to higher frequencies, which is attributed to the compressive strain in the sp^2 plane.[39] The compressive strain was induced in the CNTs at the CNT/Cu interfaces. These observations confirmed the firm contacts between the CNTs and copper, which has a smaller lattice constant.

3.3. Electrical Properties of the CNT/Cu Wire

The electrical conductivities of the mixed and unmixed CNT/Cu wires at room temperature were 1.82 × 10^5 and 3.14 × 10^4 S cm^{-1}, respectively (Figure 6a). For comparison, CNT yarn, commercial Cu wire (99.99% purity), and the international annealed copper standard (IACS) data are also plotted. The conductivity of the CNT yarn is 2.17 × 10^2 S cm^{-1}, 3 orders of magnitude lower than that of 100% IACS (5.8 × 10^5 S cm^{-1}). The conductivity of the CNT/Cu wires increased as the volume ratio of copper increased. In the linear scale plot (inset in Figure 6a), the conductivity of the mixed CNT/Cu wire was almost linear with respect to the volume fraction of copper, suggesting that the free electrons in the copper matrix were the dominant carriers. In contrast, the conductivity of the unmixed CNT/Cu wire was lower than the linear relationship. The

https://doi.org/10.1021/acsaenm.3c00269
ACS Appl. Eng. Mater. 2023, 1, 2359−2367

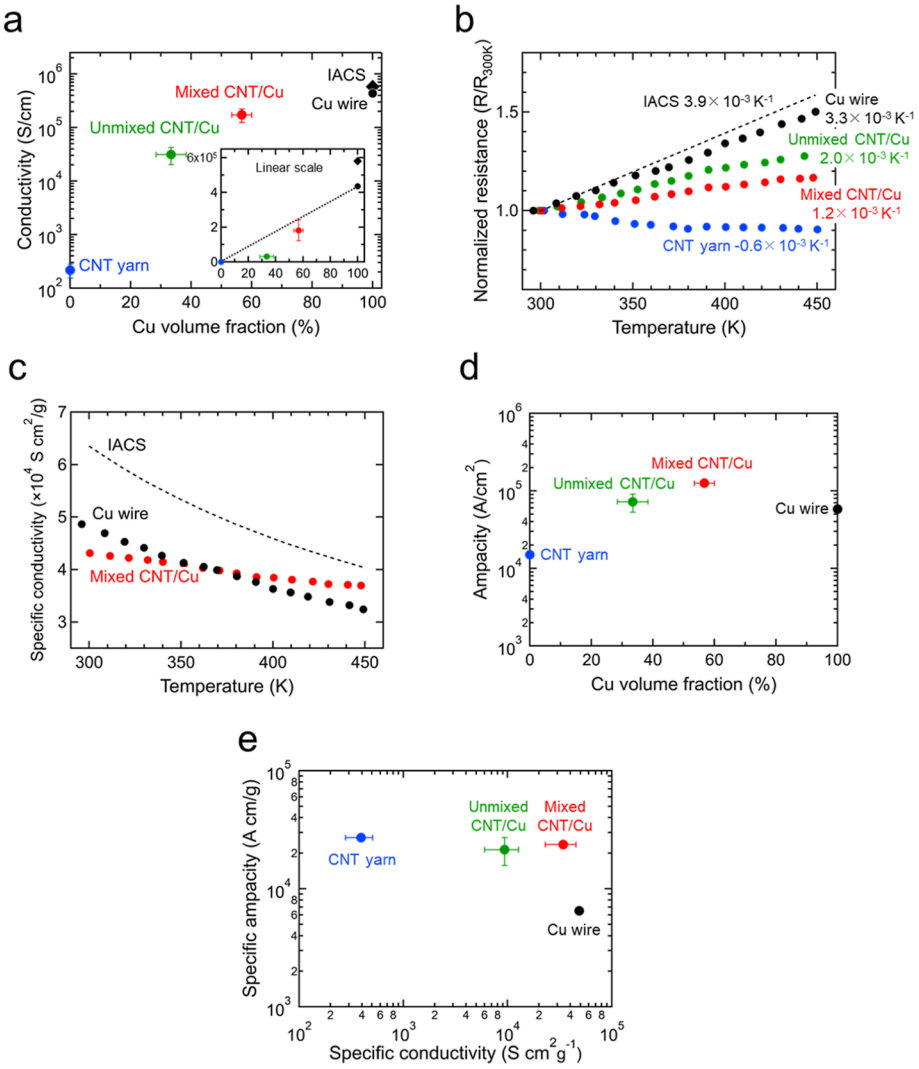

Figure 6. Electrical properties of the CNT/Cu wires, CNT yarn, commercial Cu wire, and IACS. (a) Electrical conductivity, (b) temperature dependence of resistance normalized by values at 300 K, (c) temperature dependence of the conductivity of the mixed CNT/Cu and Cu wires, and (d) ampacity. (e) Comparison of specific ampacity and specific conductivity of the samples.

cross-sectional SEM image in Figure 3c shows that copper precipitated as floating islands in the yarn, indicating that some of the copper contributed less to the conductivity, and thus, the conductivity was lower than expected from the fraction of copper.

Figure 6b shows the temperature dependence of the electrical resistance normalized by the value at 300 K. The resistance of the mixed and unmixed CNT/Cu wires increased linearly with temperature. This trend suggests that the process by which the carriers are scattered by phonons was dominant, supporting the earlier assumption that the major carriers in the composite wires were free electrons in the copper matrix. The TCRs of the mixed and unmixed wires were 1.2×10^{-3} and 2.0×10^{-3} K^{-1}, respectively, smaller than that of IACS of 3.9×10^{-3} K^{-1}. The TCR of CNT/Cu composites is reported to be smaller than that of copper in many cases.[23,29,34,40,41] Several reasons have been proposed for the lower TCR of composites of copper and nanocarbon materials. One is the mixing effect of copper and CNTs having a negative TCR.[42] The negative TCR, as obtained for the CNT yarns in this study (-0.6×10^{-3} K^{-1}), has been reported.[43−46] However, because the resistivities of copper and CNTs differ by several orders of magnitude and electrons flow through copper, the decrease in overall TCR cannot be explained by the mixture of CNTs with negative TCR.

Others have reported that elastic scattering at the interface between the Cu and graphene surfaces is a factor in the lower TCR.[47] Thus, the temperature variation of resistance is even smaller than that of the copper materials. The resistivity of CNT/Cu does not decrease substantially below the value predicted from the copper ratio, despite the large scattering cross-section due to the CNT/Cu interfaces, suggesting that the electrons do not lose kinetic energy at the interfaces. In addition, the electrical conductance of the CNT/Cu composite has been reported to be highest in the CNT alignment direction.[48] Therefore, for the aligned CNT/Cu composites, it can be concluded that the unidirectionally aligned interfaces do not act as major scattering centers for free electron transport and are more effective in suppressing phonon scattering. This explains why the mixed wire with a larger interface area than the unmixed wire had a smaller TCR.

Figure 6c compares the temperature dependence of the specific conductivities of mixed CNT/Cu, commercial Cu wires, and IACS. Due to the lower TCR of the CNT/Cu wire,

https://doi.org/10.1021/acsaenm.3c00269
ACS Appl. Eng. Mater. 2023, 1, 2359−2367

the specific conductivity exceeded that of the Cu wire above 370 K and was also expected to overtake IACS in the temperature range above 450 K. The specific conductivity of CNT/Cu composites overtaking that of copper at 100−200 °C is promising for future materials. If composites with larger interfaces are realized with even thinner CNTs, the TCR could be dramatically reduced, although the residual resistance may be somewhat larger. This would make interfacial scattering more pronounced than electron−phonon scattering, shifting the specific conductivity overtaking point to lower temperatures, and thus potentially achieving higher specific conductivity than copper even at room temperature.

The mixed CNT/Cu wire showed a high ampacity of 1.26×10^5 A cm^{-2}, which was 2.2 times higher than that of the Cu wire (5.82×10^4 A cm^{-2}) (Figure 6d). The mixed CNT/Cu wire was broken down under high current density by melting caused by Joule heating.[24,49] The specific conductivity of the CNT/Cu wire was smaller than that of copper at high temperatures above 370 K; thus, the Joule heating with the increase in current density was smaller than that of Cu wire, which mitigated the temperature rise and increased the ampacity.

Figure 6e depicts the relationship between the specific conductivity and specific ampacity of the mixed CNT/Cu wires, the CNT yarn, and the Cu wire. The specific conductivities of the mixed CNT/Cu and Cu wire were 3.42×10^4 and 4.87×10^4 S cm^2 g^{-1}, respectively. Those values were more than 2 orders of magnitude higher than those of the CNT yarn (3.92×10^2 S cm^2 g^{-1}). Because free electrons are responsible for electron transport in the CNT/Cu and Cu wires, the specific conductivities of the materials are comparable. However, the specific ampacity, which is the ampacity per weight, of the mixed CNT/Cu wire of 2.37×10^4 A cm g^{-1} was 3.6 times higher than that of 6.50×10^3 A cm g^{-1} of the Cu wire. The suppression of resistance increased at higher temperatures because the small TCR of the mixed CNT/Cu increased the specific ampacity substantially. The mixed CNT/Cu wire had higher ampacity and similar conductivity compared with copper and was 38% lighter. Thus, this material may be a candidate for thin wiring lines to provide a high power supply for integrated electronic systems.

The highest specific ampacity was obtained for the CNT yarn (2.71×10^4 A cm g^{-1}). Because the sublimation temperature of the CNT yarn is higher than that of copper and the infrared emissivity is also higher, the current was carried at higher temperatures than that of the metallic samples.[50] Therefore, even though the specific conductivity of the CNT yarn was 2 orders of magnitude smaller than that of the metallic samples, it showed a higher specific ampacity.

3.4. Mechanical Properties of the CNT/Cu Wire

The tensile properties showed a mixing effect in the mixed CNT/Cu wire. Figure 7a shows typical stress−strain curves measured on five specimens of CNT/Cu wire, CNT yarn, and Cu wire, respectively. The measured tensile properties are summarized in Table 1. The tensile strength and Young's modulus of the mixed CNT/Cu wire were 699 MPa and 70.4 GPa, respectively. These tensile properties were much higher than those of copper and CNT yarn. If the rule of mixtures is applied to the stress−strain curves, the resulting stress−strain curve of the mixed CNT/Cu wire would be located between the stress−strain curves of CNT yarn and Cu wire. This is the case for the stress−strain curve of the unmixed CNT/Cu wire,

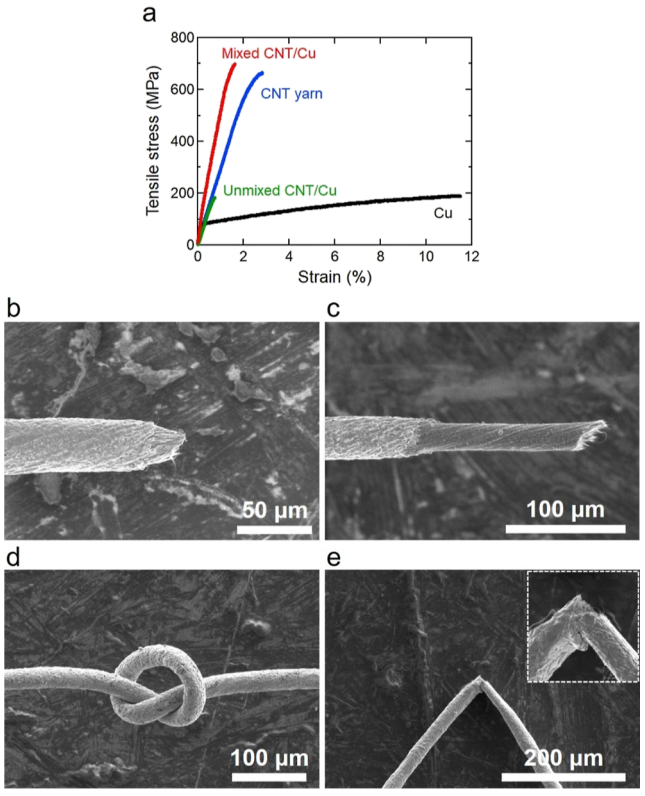

Figure 7. (a) Typical stress−strain curves of the mixed and unmixed CNT/Cu wires, the CNT yarn, and the Cu wire. Fracture images of (b) mixed and (c) unmixed CNT/Cu wires. SEM images of (d) knotted mixed CNT/Cu wire and (e) broken unmixed CNT/Cu wire.

which had a core-clad structure. These observations imply that the mixed CNT/Cu wire can be regarded as a fiber-reinforced composite, where CNTs and/or CNT bundles are the reinforcing elements, and copper is the matrix. The homogeneous mixing and firm contacts at the CNT/Cu interface provide better load transfer from the copper matrix to CNTs and CNT bundles, resulting in the excellent tensile properties of the mixed CNT/Cu wire. The experimental results and the above discussion suggest the importance of producing homogeneously mixed composite wires for CNT/Cu wires with higher tensile performance.

The fracture mechanism of the mixed and unmixed CNT/Cu wires was investigated by SEM (Figure 7b,c). For the mixed CNT/Cu wire, the tip of the fracture was elongated and necked, implying that a ductile fracture occurred similar to typical metallic materials. The observation suggests that the tensile load was uniformly distributed in the composite wire. Conversely, for the unmixed CNT/Cu wire, a long section of CNT yarn was pulled out, indicating that the copper at the periphery and inner CNT yarn were broken at different points. These results showed that in the mixed CNT/Cu wire, the copper was not only homogeneously precipitated in the CNT yarn but also adhered well to the surfaces of the CNTs and/or CNT bundles until the final fracture.

The homogeneously mixed CNT/Cu wire also had good bending properties. The mixed CNT/Cu wire deformed with a small curvature, showing high flexibility (Figure 7d). On the other hand, the unmixed CNT/Cu wire buckled and failed during bending (Figure 7e). These differences in deformation were related to the strain distribution in the composite wire

https://doi.org/10.1021/acsaenm.3c00269
ACS Appl. Eng. Mater. 2023, 1, 2359−2367

structure. The homogeneous composite structure of the mixed CNT/Cu wire dispersed stress over the entire structure. Therefore, it had both high tensile properties and flexibility. However, in the unmixed CNT/Cu wire, the CNT yarn in the center of the wire could not withstand the compressive load due to bending, and the copper clad on the surface tended to buckle. Figure 7 and the above discussion suggest the importance of producing homogeneously mixed composite wires when excellent flexibility is required.

This is the first report of a clear mixing effect in the tensile and bending properties of a composite of CNTs and copper, and our experimental results proved that homogeneous mixing and firm contacts are key to achieving higher mechanical performance in CNT/Cu wires.

4. CONCLUSIONS

We fabricated a homogeneous CNT/Cu composite wire with low TCR, high ampacity, high tensile properties, and high flexibility due to the synergistic effects between CNTs and copper. The mixed CNT/Cu wire may be suitable as a lightweight wiring material for tiny coils used in drone motors, earphones, and small actuators, and as wiring for integrated electronic device systems with high energy density. In addition, the technique of dry-spinning CNTs decorated with NPs deposited in the gas phase, which we developed to obtain homogeneous composite materials, opens up new potential applications for CNTs. Because CNTs supporting metallic NPs could be used to form various structures, such as long wires, sheets, and three-dimensional structures, it could be applied to other CNT applications with various functionalities.

■ ASSOCIATED CONTENT

Supporting Information

The Supporting Information is available free of charge at https://pubs.acs.org/doi/10.1021/acsaenm.3c00269.

Material preparation; electroplating condition; SEM images and EDS spectrum; XPS spectra of CNTs decorated with and without Cu NPs (PDF)

■ AUTHOR INFORMATION

Corresponding Author

Yoku Inoue − *Department of Electronics and Materials Science, Shizuoka University, Shizuoka 432-8561, Japan;* orcid.org/0000-0001-7701-0539; Phone: +81-53-478-1356; Email: inoue.yoku@shizuoka.ac.jp

Authors

Kosuke Tanaka − *Department of Electronics and Materials Science, Shizuoka University, Shizuoka 432-8561, Japan*

Takayuki Nakano − *Department of Electronics and Materials Science, Shizuoka University, Shizuoka 432-8561, Japan; Research Institute of Electronics, Shizuoka University, Shizuoka 432-8011, Japan*

Yoshinobu Shimamura − *Department of Mechanical Engineering, Shizuoka University, Shizuoka 432-8561, Japan*

Complete contact information is available at: https://pubs.acs.org/10.1021/acsaenm.3c00269

Notes

The authors declare no competing financial interest.

■ ACKNOWLEDGMENTS

This work was partly supported by JSPS KAKENHI grant number JP22H01521. We would like to thank Professor Nobuhisa Fujima and Associate Professor Ryo Tamura for fruitful discussions. We would also like to thank Toshiyuki Suzuki and Motoyuki Karita of JEOL for the cross-sectional TEM analysis of the samples.

■ REFERENCES

(1) Nguyen, R.T.; Eggert, R.G.; Severson, M.H.; Anderson, C.G. Global Electrification of Vehicles and Intertwined Material Supply Chains of Cobalt, Copper and Nickel. *Resour. Conserv. Recycl.* **2021**, *167*, 105198.

(2) Elshkaki, A.; Graedel, T.E.; Ciacci, L.; Reck, B. Copper demand, supply, and associated energy use to 2050. *Global Environ. Change* **2016**, *39*, 305−315.

(3) Schipper, B.W.; Lin, H.C.; Meloni, M.A.; Wansleeben, K.; Heijungs, R.; van der Voet, E. Estimating global copper demand until 2100 with regression and stock dynamics. *Resour. Conserv. Recycl.* **2018**, *132*, 28−36.

(4) Yao, Z.; Kane, C.L.; Dekker, C. High-Field Electrical Transport in Single-Wall Carbon Nanotubes. *Phys. Rev. Lett.* **2000**, *84*, 2941−2944.

(5) Wei, B.Q.; Vajtai, R.; Ajayan, P.M. Reliability and current carrying capacity of carbon nanotubes. *Appl. Phys. Lett.* **2001**, *79*, 1172−1174.

(6) Kreupl, F.; Graham, A.P.; Duesberg, G.S.; Steinhögl, W.; Liebau, M.; Unger, E.; Hönlein, W. Carbon nanotubes in interconnect applications. *Microelectron. Eng.* **2002**, *64*, 399−408.

(7) Yu, M.-F.; Lourie, O.; Dyer, M. J.; Moloni, K.; Kelly, T. F.; Ruoff, R. S. Strength and Breaking Mechanism of Multiwalled Carbon Nanotubes Under Tensile Load. *Science* **2000**, *287*, 637−640.

(8) Demczyk, B. G.; Wang, Y. M.; Cumings, J.; Hetman, M.; Han, W.; Zettl, A.; Ritchie, R. O. Direct mechanical measurement of the tensile strength and elastic modulus of multiwalled carbon nanotubes. *J. Mater. Sci. Eng. A* **2002**, *334*, 173−178. www.elsevier.com/locate/msea

(9) Zhang, M.; Atkinson, K. R.; Baughman, R. H. Multifunctional Carbon Nanotube Yarns by Downsizing an Ancient Technology. *Science* **2004**, *306*, 1358−1361.

(10) Inoue, Y.; Hayashi, K.; Karita, M.; Nakano, T.; Shimamura, Y.; Shirasu, K.; Yamamoto, G.; Hashida, T. Study on the mechanical and electrical properties of twisted CNT yarns fabricated from CNTs with various diameters. *Carbon* **2021**, *176*, 400−410.

(11) Behabtu, N.; Young, C. C.; Tsentalovich, D. E.; Kleinerman, O.; Wang, X.; Ma, A. W. K.; Bengio, E. A.; ter Waarbeek, R. F.; de Jong, J. J.; Hoogerwerf, R. E.; Fairchild, S. B.; Ferguson, J. B.; Maruyama, B.; Kono, J.; Talmon, Y.; Cohen, Y.; Otto, M. J.; Pasquali, M. Strong, Light, Multifunctional Fibers of Carbon Nanotubes with Ultrahigh Conductivity. *Science* **2013**, *339*, 182−186.

(12) Koziol, K.; Vilatela, J.; Moisala, A.; Motta, M.; Cunniff, P.; Sennett, M.; Windle, A. High-Performance Carbon Nanotube Fiber. *Science* **2007**, *318*, 1892−1895.

(13) Li, Q.; Li, Y.; Zhang, X.; Chikkannanavar, S. B.; Zhao, Y.; Dangelewicz, A. M.; Zheng, L.; Doorn, S. K.; Jia, Q.; Peterson, D. E.; Arendt, P. N.; Zhu, Y. Structure-dependent electrical properties of carbon nanotube fibers. *Adv. Mater.* **2007**, *19*, 3358−3363.

(14) Jakubinek, M. B.; Johnson, M. B.; White, M. A.; Jayasinghe, C.; Li, G.; Cho, W.; Schulz, M. J.; Shanov, V. Thermal and electrical conductivity of array-spun multi-walled carbon nanotube yarns. *Carbon* **2012**, *50*, 244−248.

(15) Zhang, S.; Zhu, L.; Minus, M. L.; Chae, H. G.; Jagannathan, S.; Wong, C. P.; Kowalik, J.; Roberson, L. B.; Kumar, S. Solid-state spun fibers and yarns from 1-mm long carbon nanotube forests synthesized by water-assisted chemical vapor deposition. *J. Mater. Sci.* **2008**, *43*, 4356−4362.

(16) Miao, M.; McDonnell, J.; Vuckovic, L.; Hawkins, S. C. Poisson's ratio and porosity of carbon nanotube dry-spun yarns. *Carbon* **2010**, *48*, 2802−2811.
(17) Aliev, A. E.; Guthy, C.; Zhang, M.; Fang, S.; Zakhidov, A. A.; Fischer, J. E.; Baughman, R. H. Thermal transport in MWCNT sheets and yarns. *Carbon* **2007**, *45*, 2880−2888.
(18) Miao, M. Electrical conductivity of pure carbon nanotube yarns. *Carbon* **2011**, *49*, 3755−3761.
(19) Zhang, X.; Li, Q.; Tu, Y.; Li, Y.; Coulter, J. Y.; Zheng, L.; Zhao, Y.; Jia, Q.; Peterson, D. E.; Zhu, Y. Strong carbon-nanotube fibers spun from long carbon-nanotube arrays. *Small* **2007**, *3*, 244−248.
(20) Taylor, L. W.; Dewey, O. S.; Headrick, R. J.; Komatsu, N.; Peraca, N. M.; Wehmeyer, G.; Kono, J.; Pasquali, M. Improved properties, increased production, and the path to broad adoption of carbon nanotube fibers. *Carbon* **2021**, *171*, 689−694.
(21) Sundaram, R. M.; Sekiguchi, A.; Sekiya, M.; Yamada, T.; Hata, K. Copper/carbon nanotube composites: Research trends and outlook. *R. Soc. Open Sci.* **2018**, *5*, 180814.
(22) Janas, D.; Liszka, B. Copper matrix nanocomposites based on carbon nanotubes or graphene. *Mater. Chem. Front.* **2018**, *2*, 22−35.
(23) Subramaniam, C.; Yamada, T.; Kobashi, K.; Sekiguchi, A.; Futaba, D. N.; Yumura, M.; Hata, K. One hundred fold increase in current carrying capacity in a carbon nanotube-copper composite. *Nat. Commun.* **2013**, *4*, 2202.
(24) Bazbouz, M. B.; Aziz, A.; Copic, D.; de Volder, M.; Welland, M. E. Fabrication of High Specific Electrical Conductivity and High Ampacity Carbon Nanotube/Copper Composite Wires. *Adv. Electron. Mater.* **2021**, *7*, 2001213.
(25) Arai, S.; Murakami, I.; Shimizu, M.; Oshigane, A. Fabrication of CNT/Cu Composite Yarn via Single-Step Electrodeposition. *J. Electrochem. Soc.* **2020**, *167*, 102509.
(26) Hannula, P. M.; Peltonen, A.; Aromaa, J.; Janas, D.; Lundström, M.; Wilson, B. P.; Koziol, K.; Forsén, O. Carbon nanotube-copper composites by electrodeposition on carbon nanotube fibers. *Carbon* **2016**, *107*, 281−287.
(27) Park, M.; Lee, D. M.; Park, M.; Park, S.; Lee, D. S.; Kim, T. W.; Lee, S. H.; Lee, S. K.; Jeong, H. S.; Hong, B. H.; Bae, S. Performance enhancement of graphene assisted CNT/Cu composites for light-weight electrical cables. *Carbon* **2021**, *179*, 53−59.
(28) Daneshvar, F.; Chen, H.; Zhang, T.; Sue, H. J. Fabrication of Light-Weight and Highly Conductive Copper−Carbon Nanotube Core−Shell Fibers Through Interface Design. *Adv. Mater. Interfaces* **2020**, *7*, 2000779.
(29) Zou, J.; Liu, D.; Zhao, J.; Hou, L.; Liu, T.; Zhang, X.; Zhao, Y.; Zhu, Y. T.; Li, Q. Ni Nanobuffer Layer Provides Light-Weight CNT/Cu Fibers with Superior Robustness, Conductivity, and Ampacity. *ACS Appl. Mater. Interfaces* **2018**, *10*, 8197−8204.
(30) Han, B.; Guo, E.; Xue, X.; Zhao, Z.; Li, T.; Xu, Y.; Luo, L.; Hou, H. Fabricating and strengthening the carbon nanotube/copper composite fibers with high strength and high electrical conductivity. *Appl. Surf. Sci.* **2018**, *441*, 984−992.
(31) Han, B.; Guo, E.; Xue, X.; Zhao, Z.; Luo, L.; Qu, H.; Niu, T.; Xu, Y.; Hou, H. Fabrication and densification of high performance carbon nanotube/copper composite fibers. *Carbon* **2017**, *123*, 593−604.
(32) Wang, G. J.; Ma, Y. J.; Cai, Y. P.; Cao, Z. H.; Meng, X. K. Overcoming the strength-conductivity trade-off dilemma in carbon nanotube/aluminum-copper fibers by diffusion interface and chemical reaction interface. *Carbon* **2019**, *146*, 293−300.
(33) Bazbouz, M. B.; Aziz, A.; Copic, D.; de Volder, M.; Welland, M. E. Fabrication of High Specific Electrical Conductivity and High Ampacity Carbon Nanotube/Copper Composite Wires. *Adv. Electron. Mater.* **2021**, *7*, 2001213.
(34) Sundaram, R.; Yamada, T.; Hata, K.; Sekiguchi, A. Electrical performance of lightweight CNT-Cu composite wires impacted by surface and internal Cu spatial distribution. *Sci. Rep.* **2017**, *7*, 9267.
(35) Kinoshita, T.; Karita, M.; Nakano, T.; Inoue, Y. Two step floating catalyst chemical vapor deposition including in situ fabrication of catalyst nanoparticles and carbon nanotube forest growth with low impurity level. *Carbon* **2019**, *144*, 152−160.
(36) Kinoshita, T.; Karita, M.; Chikyu, N.; Nakano, T.; Inoue, Y. Enhancement of catalytic activity by addition of chlorine in chemical vapor deposition growth of carbon nanotube forests. *Carbon* **2022**, *196*, 391−400.
(37) Ghemes, A.; Minami, Y.; Muramatsu, J.; Okada, M.; Mimura, H.; Inoue, Y. Fabrication and mechanical properties of carbon nanotube yarns spun from ultra-long multi-walled carbon nanotube arrays. *Carbon* **2012**, *50*, 4579−4587.
(38) Lima, M. D.; Fang, S.; Lepró, X.; Lewis, C.; Ovalle-Robles, R.; Carretero-González, J.; Castillo-Martínez, E.; Kozlov, M. E.; Oh, J.; Rawat, N.; Haines, C. S.; Haque, M. H.; Aare, V.; Stoughton, S.; Zakhidov, A. A.; Baughman, R. H. Biscrolling Nanotube Sheets and Functional Guests into Yarns. *Science* **2011**, *331*, 51−55.
(39) Lee, J. E.; Ahn, G.; Shim, J.; Lee, Y. S.; Ryu, S. Optical separation of mechanical strain from charge doping in graphene. *Nat. Commun.* **2012**, *3*, 1024.
(40) Leggiero, A. P.; Trettner, K. J.; Ursino, H. L.; McIntyre, D. J.; Schauer, M.; Zeira, E.; Cress, C. D.; Landi, B. J. High Conductivity Copper−Carbon Nanotube Hybrids via Site-Specific Chemical Vapor Deposition. *ACS Appl. Nano Mater.* **2019**, *2*, 118−126.
(41) Sun, S.; Mu, W.; Edwards, M.; Mencarelli, D.; Pierantoni, L.; Fu, Y.; Jeppson, K.; Liu, J. Vertically aligned CNT-Cu nanocomposite material for stacked through-silicon-via interconnects. *Nanotechnology* **2016**, *27*, 335705.
(42) Lee, S.; Kim, E.-M.; Lim, Y. Near-zero temperature coefficient of resistance of hybrid resistor fabricated with carbon nanotube and metal alloy. *Sci. Rep.* **2019**, *9*, 7763.
(43) Niven, J. F.; Johnson, M. B.; Juckes, S. M.; White, M. A.; Alvarez, N. T.; Shanov, V. Influence of annealing on thermal and electrical properties of carbon nanotube yarns. *Carbon* **2016**, *99*, 485−490.
(44) Bhatia, R.; Prasad, V.; Menon, R. Probing the inter-tube transport in aligned and random multiwall carbon nanotubes. *J. Appl. Phys.* **2011**, *109*, 053713.
(45) Bekyarova, E.; Itkis, M. E.; Cabrera, N.; Zhao, B.; Yu, A.; Gao, J.; Haddon, R. C. Electronic properties of single-walled carbon nanotube networks. *J. Am. Chem. Soc.* **2005**, *127*, 5990−5995.
(46) Yanagi, K.; Udoguchi, H.; Sagitani, S.; Oshima, Y.; Takenobu, T.; Kataura, H.; Ishida, T.; Matsuda, K.; Maniwa, Y. Transport mechanisms in metallic and semiconducting single-wall carbon nanotube networks. *ACS Nano* **2010**, *4*, 4027−4032.
(47) Mehta, R.; Chugh, S.; Chen, Z. Enhanced Electrical and Thermal Conduction in Graphene-Encapsulated Copper Nanowires. *Nano Lett.* **2015**, *15*, 2024−2030.
(48) Ghorbani-Asl, M.; Bristowe, P. D.; Koziol, K. A computational study of the quantum transport properties of a Cu−CNT composite. *Phys. Chem. Chem. Phys.* **2015**, *17*, 18273−18277.
(49) Subramaniam, C.; Yamada, T.; Kobashi, K.; Sekiguchi, A.; Futaba, D. N.; Yumura, M.; Hata, K. One hundred fold increase in current carrying capacity in a carbon nanotube-copper composite. *Nat. Commun.* **2013**, *4*, 2202.
(50) Sugime, H.; Sato, T.; Nakagawa, R.; Hayashi, T.; Inoue, Y.; Noda, S. Ultra-long carbon nanotube forest via in situ supplements of iron and aluminum vapor sources. *Carbon* **2021**, *172*, 772−780.

https://doi.org/10.1021/acsaenm.3c00269
ACS Appl. Eng. Mater. 2023, 1, 2359−2367